The 8th TSME International Conference on Mechanical Engineering
12-15 December 2017
Bangkok, Thailand

TSF0005

Multi-flow modes between co-rotating disks in casing by numerical analysis and experiment

R. Uenishi[1], T. Watanabe[2], H. Tanigawa[3], and K. Hirata[1,*]

1 Department of Mechanical Engineering, Doshisha University, Kyoto 610-0321, Japan
2 Department of Information Science, Nagoya University, Nagoya 464-8601, Japan
3 Department of Mechanical Engineering, NIT Maizuru College, Maizuru 625-0016, Japan

* Corresponding Author: khirata@mail.doshisha.ac.jp

Abstract. The authors consider the flow between co-rotating disks, namely, the disks which rotate co-axially in the same direction at the same angular velocity, with a narrow gap enclosed by a stationary shroud at their circumferences. The flow often accompanies azimuthally-fluctuating instabilities; a non-axisymmetric secondary flow nears the shroud. In this study, the authors experimentally and numerically research the flow in torus-vortex modes, in addition to core-shape modes. Specifically speaking, in experiments, the authors visualise the meridian plane (r-θ plane) and the midplane (r-z plane) between co-rotating disks, using a high-speed video camera and a YAG laser to carry out particle-image-velocimetry (PIV) analyses. Based on such PIV results, the torus-vortex modes and the core-shape modes are defined. On the basis of many experimental and numerical observations, the authors report stability diagrams to predict their occurrence and criteria for their frequencies. Furthermore, authors discuss the relation between the flow modes.

1. Introduction

The flow in the neighborhood of a rotating disk is of practical importance, particularly in connection with rotary machines (Schlichting, 1979 [1]) common in turbo-machineries. The flow on a single infinite rotating disk or the flow between two infinite coaxially rotating disks have been studied by many researchers [2 – 6]. Then, the flow around a single and shrouded rotating disks with a finite radius and the flow between two finite co-axial rotating disks have been studied as well [7 – 11]. These flow problems can be found out in various fundamental industrial applications such as axial compressors, vane less diffusers, multiple-disk pumps and disk/drum-brake systems. In general, these types of flow tend to include non-axisymmetric secondary flows known as 'stall propagations' which occasionally cause disk vibrations and noises [12 – 15].

Now, we consider the flow between two co-rotating disks which rotate co-axially in the same direction at the same angular velocity with a narrow gap enclosed by a stationary shroud (or a stationary casing) at their circumferences. This flow is modelled on the flow inside the random-access disk-storage device of computers. The flow has been studied by many researchers [16 – 27], because, the flow is very complicated with three-dimensionality and turbulence. For example, when we visualise the flow on a plane between the disks (or the r-θ plane), we often see an azimuthally-fluctuating instability which exhibits a non-axisymmetric secondary flow near the stationary shroud with a clear boundary. The clear boundary exists between the core region which is the laminar-flow region around the central hub and the outer region where the flow is turbulent near the stationary shroud. This clear boundary, hereinafter, referred to as a core boundary, between the core region and the outer region has a near-polygonal shape, such as hexagon, pentagon, square, triangle and ellipse, together with circle. The core-boundary shape rotates slightly slower than the disks, while the fluid in the core region rotates in a rigidly-rotational motion with the disks. On the other hand, when we visualise the flow in the meridional plane (or the r-z plane), we often see a pair of torus-vortex structures near the stationary shroud.

In the present study, focusing upon the core-boundary shape, we classify the azimuthally-fluctuating instability observed on the midplane between the disks (or the middle r-θ plane) into six flow modes as a function of the Reynolds number Re and two geometric parameters δ and κ. Hereinafter, these flow modes are referred to as core-shape modes CSMs. Furthermore, we also focus upon the other flow modes called as torus-vortex modes TVMs, in addition to CSMs. Then we conduct experiment and numerical analysis on the flow. And, we reveal the stability diagrams concerning both CSMs and TVMs of the flow. Especially in computations, we compare computational results with experimental results, and try to reveal the details of flow structure in each mode.

2. Methodology

Figure 1 shows a side view of the present model. The model is composed of two coaxial rotating disks, cylindrical hub between them and a stationary peripheral shroud. The disks rotate in the same direction at the same angular velocity Ω_d with a narrow spacing G. In the present study, as non-dimensional system parameters, we choose a disk-tip Reynolds number $Re \equiv \Omega_d R_d^2/\nu$, a gap aspect ratio $\delta \equiv G/R_d$, a non-dimensional hub radius $\kappa \equiv R_h/R_d$ and a non-dimensional peripheral radius $\lambda \equiv R_w/R_d$, where R_d and R_h are the radii of the rotating disk and the hub, respectively. Characteristic velocity is a disk-tip velocity $R_d\Omega_d$. Tables 1 and 2 summarise the present experimental and computational parameters, respectively.

In experiments, we visualise both the midplane and the meridional plane, using a high-speed video camera and a YAG laser to carry out particle-image-velocimetry (referred to as PIV) analysis. For flow visualisation, the upper disk and the cylindrical container are transparent and the others are frosted. The flow between the disks is visualised using SiO_2 particles coated by fluorescent paint, and it is recorded by a high-speed video camera above the disks for top view or beside the disks for side view.

In computations, we assume that Mach number Ma is much smaller than unity. Therefore, fluid is supposed to be incompressible. So, the governing equations are the incompressible unsteady Navier-Stokes equations and the equation of continuity. These governing equations in a cylindrical coordinate system are solved by a finite difference method based on the MAC method for the coupling between $\boldsymbol{v}$ and p with the FTCS scheme using a staggered grid system.

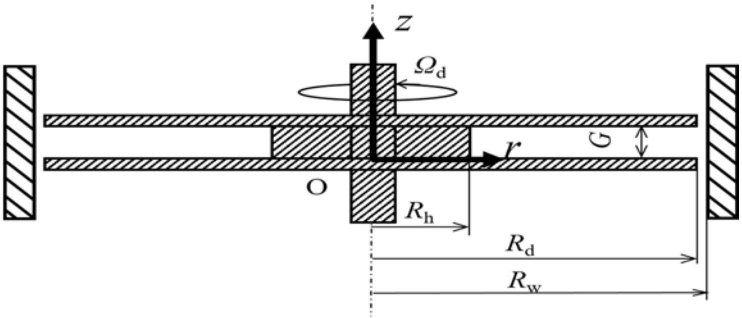

G : Gap
R_d : Radius of rotating disk (= 153 mm)
R_h : Radius of hub
R_w : Radius to stationary shroud's wall (= 155 mm)
Ω_d : Angular velocity of disk rotation, $= 2\pi/T_d$

Figure 1. Model, together with experimental parameters and coordinate system.

Table 1. Experimental parameters.

Disk-trip Reynolds number Re ($\equiv \Omega_d R_d^2/\nu$)	$1.4\times10^3 - 1.4\times10^5$
Gap aspect ratio δ ($\equiv G/R_d$)	0.10 – 0.30
Non-dimensional hub radius κ($\equiv R_h/R_d$)	0.11
Non-dimensional enclosure radius λ ($\equiv R_w/R_d$)	$1.01 \approx 1.0$

Table 2. Computational parameters.

Disk-trip Reynolds number Re ($\equiv \Omega_d R_d^2/\nu$)	$1.4\times10^3 - 1.4\times10^4$
Gap aspect ratio δ ($\equiv G/R_d$)	0.10 – 0.30
Non-dimensional hub radius κ($\equiv R_h/R_d$)	0.11
Non-dimensional enclosure radius λ ($\equiv R_w/R_d$)	$1.01 \approx 1.0$

3. Results and Discussion

3.1. Time-mean flow

First of all, we examine (time-)mean flow, which has an axisymmetric structure in space. Figure 2 shows an example of computational results: namely, radial profiles of mean velocities $\bar{v}_r$, $\bar{v}_\theta$ and $\bar{v}_z$ on the midplane (on the r-θ plane at z/G = 0.50), together with the experiment (a dashed line in the figure) and the computation (a chained line in the figure) by Humphrey *et al*. (1995) [21] whose Re and κ are larger than the present ones. A superscript " $\bar{\ }$ " represents to be time-mean over enough long time. A blue solid line in the figure denotes $\bar{v}_\theta$ in the rigid rotation like $\bar{v}_\theta = r\Omega_d$.

We can see that the fluid in such a wide inner region as $r/R_d \lesssim 0.8$ is approximately in a rigidly-rotational motion with the disks. On the other hand, in such a narrow outer region as $r/R_d \gtrsim 0.8$, the mean flow is three-dimensional and seems complicated. Besides, we can see that the present result almost agrees with Humphery *et al*.

Figure 3 shows the flow on the meridional plane (the r-z plane); that is, the distributions of mean velocities $\bar{v}_r$ in panel (a), $\bar{v}_\theta$ in panel (b) and $\bar{v}_z$ in panel (c). In the inner region as $r/R_d \lesssim 0.8$, $\bar{v}_r$ and $\bar{v}_z$ are almost zero, everywhere. And, $\bar{v}_\theta$ is constant in the z direction, depending on r/R_d. Again, we can confirm that the fluid in the inner region is approximately in a rigid rotation. In the outer region at

$r/R_\mathrm{d} \gtrsim 0.8$, we see two centrifugal currents at $z/G \approx 0.2$ and 0.8 and one centripetal current at $z/G \approx 0.5$ in panel (a). As well, we see a pair of midplane-ward concentrating currents from the disks at $r/R_\mathrm{d} \approx 0.95$ and a pair of disk-ward spreading currents from the midplane at $r/R_\mathrm{d} = 0.8 - 0.9$ in panel (c). So, we can recognise a pair of torus vortices in the outer region.

3.2. Core-shape mode

In this subsection, we define the core-shape mode CSM. Figure 4 shows the distributions of axial-vorticity component ζ_z on the midplane by experiments (PIV analysis). Panels (a) – (g) are related with seven different *Re* and gap aspect ratio δ. And, we should note that the figures represent not mean but instantaneous flow at an instant. In figure 4, we can confirm a distinct boundary between an inner region at $r/R_\mathrm{d} \lesssim 0.6 - 0.8$ and an outer region near the shroud at $r/R_\mathrm{d} \gtrsim 0.6 - 0.8$. We hereinafter refer to the inner region as "core region" and the distinct boundary's geometry as "core shape." In core region, ζ_z is almost twice Ω_d. So, in the core region, fluid is almost in a rigidly-rotational motion with Ω_d at any instant in any conditions, as well as mean flow shown in figures 2 and 3.

In each panel in figure 4, we can see that the core shape is a nearly-polygonal. For further discussion, we now define the core-shape mode CSMs corresponding to the number of polygonal vertices of the boundary. For example, in Fig. 4(c), we can identify CSM6 because the boundary shape is hexagonal.

By computations as well as experiments, we successfully identify these CSMs.

3.3. Torus-vortex mode

Based on the vortices' structure in outer region on the meridional plane (the *r*-*z* plane), we classify the flow as follows.

TVM1: A pair of torus vortices are steady, axisymmetric and symmetric about the midplane.

TVM1A: A pair of torus vortices cyclically and alternately expand and contract mainly in the axial direction on a meridional plane.

TVM1B: Remarkable features are similar with TVM1A, but the dominant directions of vortices' expansion/contraction are not only axially but also radially.

TVM2: A pair of torus vortices are steady and axisymmetric, but asymmetric about the midplane.

TVM2B: As well as TVM2, a pair of vortices remain asymmetric. However, the vortices are not steady but unsteady, expanding/contracting axially and radially.

TVM3: It is hard to confirm a pair of torus vortices, clearly. Fluctuations of the vortices are not periodic, but random.

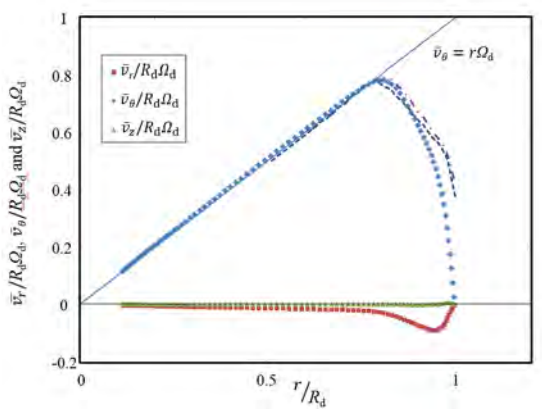

Figure 2. Radial profiles of mean velocity components (for $Re = 2.7\mathrm{x}10^3$, $\delta = 0.10$, $\kappa = 0.11$, $\lambda = 1.0$ and $z/G = 0.50$ by computation).

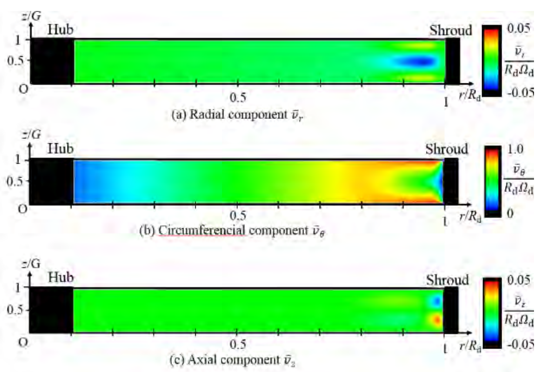

Figure 3. Distributions of mean velocity on the meridional plane (for $Re = 2.7\mathrm{x}10^3$, $\delta = 0.10$, $\kappa = 0.11$ and $\lambda = 1.0$ by computation)

As an example of TVMs, figure 5 shows the distributions of circumferential-vorticity component ζ_θ in TVM2B by experiment. Of course, we have confirmed that computational results well correspond to the experimental ones. In figure 5, positive and negative vortex structures are asymmetric about the midplane and unsteady.

3.4. Stability diagram

Now, we reveal the stability diagram concerning both the core-shape modes CSMs and the torus-vortex modes TVMs, for the non-dimensional hub radius κ = 0.11 and λ =1.0 in wide ranges of other two system parameters of the disk-tip Reynolds number *Re* and the gap aspect ratio δ.

Figure 6 shows a stability diagram of CSMs and TVMs on the *Re*-δ space. Green zones represent each CSMs stable region and blank zones by experiment between the green zones show transition regions where we could not determine CSM. Also, red solid lines denote the border between TVMs stable regions by experiment.

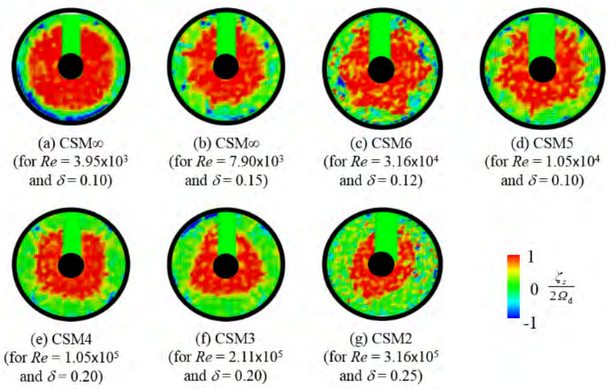

Figure 4. Core-shape modes CSM's: distributions of vorticity ζ_z on the midplane between disks (on the r-θ plane at z/G = 0.50 for κ = 0.11 and λ =1.0 by experiment).

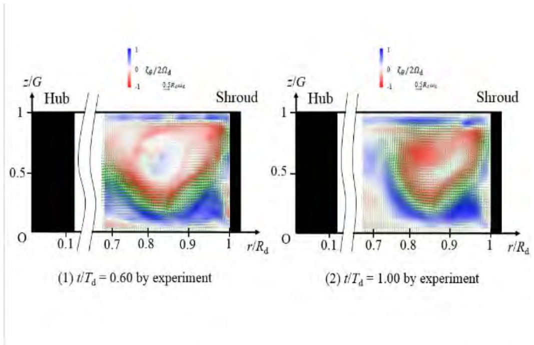

Figure 5. Distributions of vorticity denseness on the meridional plane (r-z plane) in time sequence (for *Re* = 5.4x10^3 and δ = 0.3 in TVM2B by experiment)

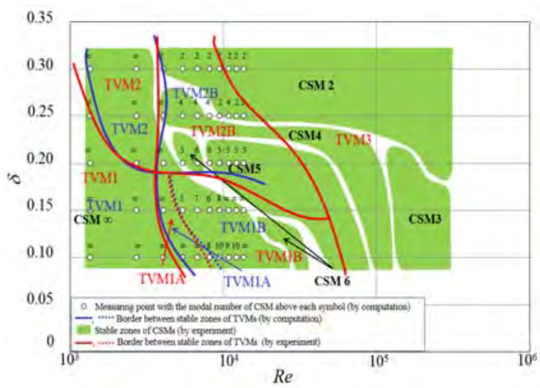

Figure 6. Stability diagram of both core-shape modes CSM∞ – CSM2 and torus-vortex modes TVM1 – TVM3 (for κ = 0.11 and λ = 1.0 by experiment and computation).

About CSMs, the increases of *Re* and δ tend to decrease the modal number of CSM. About TVMs, the increases of *Re* is apt to enhance the irregularity of the TVM (axisymmetry, unsteadiness and periodicity). The increase of δ influences the asymmetry about midplane. The increase of the *Re* promotes the non-axisymmetry of TVM 2 and TVM 2B, the aperiodicity of TVM 3 and the amplitude of the periodic oscillation of TVM 1A, TVM 1B and TVM 2B. The parameter δ has the influences similar to that of *Re*.

For reference, figure 6 shows the comparison between the numerical result and the experimental result on the stability diagram of CSMs and TVMs for λ =1.0 and κ = 0.11. The number above each symbol denotes the modal number of CSM and blue solid lines denote the border between TVMs stable regions in computation. The Green regions and the red solid lines are the same as those in figure 7. In figure 8, the boundary between TVM1A and 1B or TVM 2 and 2B exists near the boundary where CSM's modal number changes from ∞ to some number. So it is considered that the torus vortex structure became unsteady when core shape changes from circular to polygonal, because CSM's modal number shows the number of core vertices and these boundary between TVMs relate to the magnitude of radial fluctuation of torus vortex structures.

As a result, we can see good agreement between the experimental and computational results concerning both CSM and TVM in figure 6.

3.5. Three-dimensional flow structure

Numerical analysis is useful to investigate the concerning flow in detail. In general, it is difficult to estimate numerical accuracy for non-linear phenomena such as the cornering flow. However, we have confirmed it by the comparison with experimental results.

In order to examine three dimensional structure of the concerning flow, we visualize the flow to use second invariant of Q velocity-gradient tensor. Figures 9 – 12 show some examples obtained by computation to visualise the whole three-dimensional structures of the concerning flows.

At first, figure 7 exhibits the flow at $Re = 1.4\text{x}10^3$, $\delta = 0.10$, $\kappa = 0.11$ and $\lambda = 1.0$. The flow is in CSM∞ and TVM1. Then, the flow is in axsymmetry, steady and in the symmetry about midplane. This well corresponds to figure 7. Second, figure 8 presents the flow at $Re = 2.7\text{x}10^3$, $\delta = 0.30$, $\kappa = 0.11$ and $\lambda = 1.0$. The flow is in CSM∞ and TVM2. Then, the flow is in axsymmetry and steady, but in asymmetry about midplane in contrast with figure 7. Thirdly, figure 9 represents the flow at $Re = 4.1\text{x}10^3$, $\delta = 0.15$, $\kappa = 0.11$ and $\lambda = 1.0$. The flow is in CSM∞ and TVM1A. In outer region, we can find a pair of azimuthally-fluctuating torus vortices with a constant interval between neighboring nodes. These torus vortices rotate in the same direction as disks with lower angular velocity than disks'. This flow structure in the outer region is known as the shift-and-reflect symmetry reported by Herero et al. (1999). Finally, figure 10 exhibits the flow at $Re = 8.2\text{x}10^3$, $\delta = 0.15$, $\kappa = 0.11$ and $\lambda = 1.0$. The flow is in CSM6 and TVM1B. In contrast with TVM1A, the flow is disturbed in radial direction. Besides, the core has an almost hexagonal boundary, and the fluid inside the core is in the rigid rotation with disks. In this figure, disks, the core boundary and the outer-region vortical structures rotate not with the same speed but with three different speeds. This will be discussed in the next section.

3.6. Rotation speeds of core shape and outer vortices

In order to investigate the rotation speeds of the core-boundary vertex and the outer-region vortical structure more precisely, we introduce two inspection conditions IC1 and IC2. IC1 is to reveal the *Re*'s effect, and IC2 is to reveal the δ's effect. Namely, in IC1, $(Re, \delta) = (6.8\text{x}10^3 – 1.2\text{x}10^4, 0.10)$, and in IC2, (Re, δ) = (about $5\text{x}10^3$ (to be strict, $4.1\text{x}10^3 – 6.8\text{x}10^3$), 0.10 – 0.30).

Figures 11 and 12 show non-dimensional angular velocities ω_c/Ω_d of the core shape and ω_o/Ω_d of outer-vortices. Figure 11 and 12 are in IC1 and IC2, respectively.

In figure 11, $\omega_c/\Omega_d \approx 0.85$, except for $Re = 5.5\text{x}10^3$ where $\omega_c/\Omega_d \approx 0.6$. And, ω_o/Ω_d is always constant to about 0.6, being independent of *Re*. Now, we assume that ω_c and ω_o are intrinsically about 0.85 and 0.6, respectively. Under this assumption, we can regard that ω_c synchronises with ω_o for $Re = 5.5\text{x}10^3$, and that ω_c does not synchronise with ω_o for $Re > 5.5\text{x}10^3$. Hereinafter, the former is referred to as "low-ω-synchronisation," and the latter is referred to as "anti-synchronisation."

In figure 12, $\omega_c/\Omega_d \approx 0.6$, except for $\delta = 0.20$ where $\omega_c/\Omega_d \approx 0.85$. And, ω_o/Ω_d always coincides with ω_c/Ω_d, being independent of δ. So, the low-ω-synchronisation appears except for $\delta = 0.20$. For $\delta = 0.20$, we can consider that ω_o/Ω_d synchronises with ω_c/Ω_d. Hereinafter, this is referred to as "high-ω-synchronisation."

Figure 13 shows the appearance concerning the high-ω-synchronisation, the low-ω-synchronisation and anti-synchronisation on the *Re*-δ plane, together with the stability diagrams of CSMs and TVMs. Either of the high-ω-synchronisation or the anti-synchronisation appears, when the flow is unsteady. And, the high-ω-synchronisation is exceptional. These results suggest that the slower-rotational motion with about $0.6\Omega_d$ is usually observed. And, in addition to the slower rotational motion, the faster-rotation motion with about $0.85\Omega_d$ tends to be observed, when the flow is in TVM1B which is possibly linked to the complexity of the CSMs.

Furthermore, mean velocity $\bar{v}_\theta$ at the center of the outer-region is close to $0.6R_d\Omega_d$ as shown in figure 2. This seems acceptable, if we suppose the vortical structures in the outer-region advect with an average speed of the outer-region. This supports such an assumption as ω_c and ω_o are trinsically around 0.85 and 0.6, respectively.

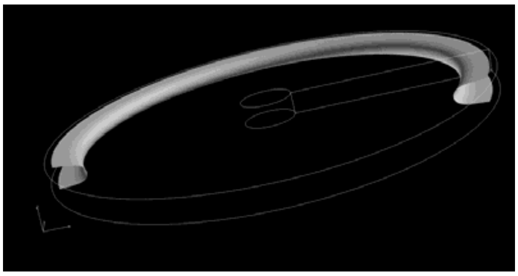

Figure 7. Iso-surfaces for Q = 0.75 at an instant in CSM∞ and TVM1 at $Re = 1.4\text{x}10^3$, δ = 0.10, κ = 0.11 and λ = 1.0 by computation.

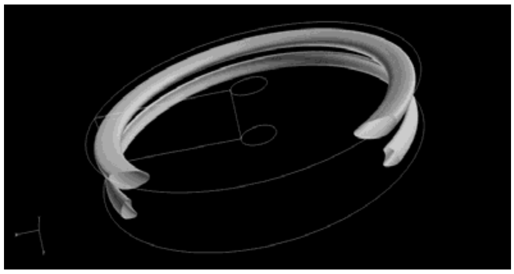

Figure 8. Iso-surfaces for Q = 1.5 at an instant in CSM∞ and TVM2 at $Re = 2.7\text{x}10^3$, δ = 0.30, κ = 0.11 and λ = 1.0 by computation.

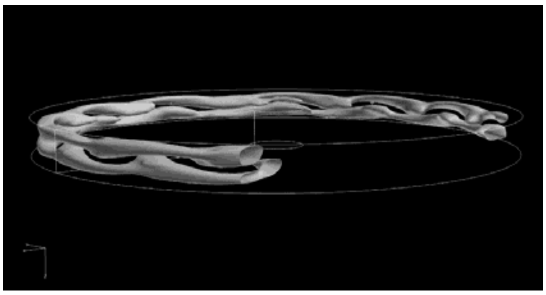

Figure 9. Iso-surfaces for Q = 1.5 at an instant in CSM∞ and TVM1A at $Re = 4.1\text{x}10^3$, δ = 0.15, κ = 0.11 and λ = 1.0 by computation.

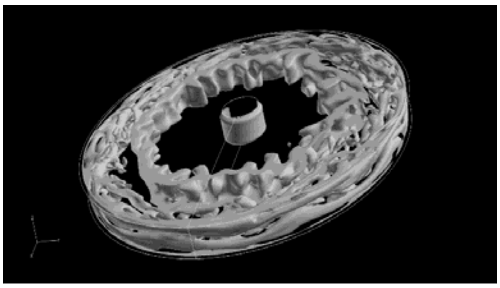

Figure. 10. Iso-surfaces for Q = 2.0 at an instant in CSM6 and TVM1B at $Re = 8.2\text{x}10^3$, δ = 0.15, κ = 0.11 and λ = 1.0 by computation.

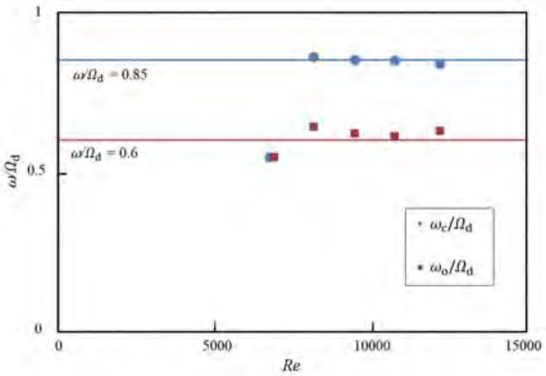

Figure 11. Non-dimensional angular velocities of core-boundary and outer-vortex in IC1 (for Re = 6800 – 12240 and δ = 0.10 by computation).

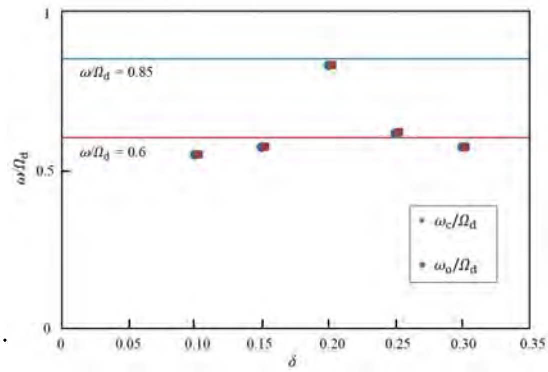

Figure 12. Non-dimensional angular velocity of core-boundary and outer-vortex in IC2 (for $Re \approx$ 5000(4080 – 6800) and δ = 0.10 – 0.30 by computation).

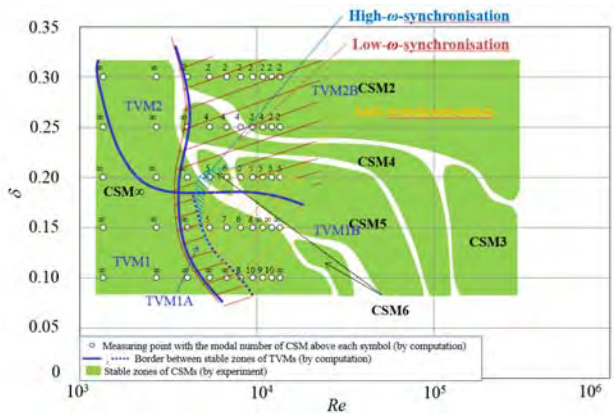

Figure 13. Appearance concerning high-ω-synchronisation, low-ω-synchronisation and anti-synchronisation, together with stability diagrams of CSMs and TVMs (for κ = 0.11 and λ = 1.0 by computation).

4. Conclusion

Obtained results are as follows.

1. In the inner region within 70 – 80% of the disk radius, the flow rotates almost rigidly with the disk.
2. Core shape mode CSM and torus vortex mode TVM are classified into six types.
3. The increases of Re and δ tend to decrease the modal number of CSM.
4. About TVMs, the increases of Re is apt to enhance the irregularity (axisymmetry, unsteadiness and periodicity) and the increase of δ influences the asymmetry about midplane.
5. The torus vortex structure became unsteady when core shape changes from circular to polygonal.
6. The experimental and computational results concerning both CSM and TVM agree well..
7. Angular velocity in the core region ω_c and outer region ω_o are intrinsically around 0.85 and 0.6, respectively

References

[1] Schlichtuig, H., 1979. *Boundary-Layer Theory, 7th edition,* MacGrow-Hill, New York, 647 – 652.
[2] Karman, T. von, 1921, Uber laminare and turbulente reibung. *Z. Ang. Math. Mech.*, **1**, 1325 – 1336.
[3] Cochran, W. G., 1934, The flow due to a rotating disk. *Proc. Cambridge Philos. Soc.*, **10**, 465 – 491.
[4] Batchelor, G. K., 1951, Note on a class of solutions of the Navier-Stokes equations representing steady rotationally-symmetric flow. *Quarterly J. of Mech. And Appl. Math.*, **4**, 29 – 41.
[5] Stewartoson, K., 1953, On the flow between two rotating coaxial disks. *Proc. Cambridge Phil. Soc.*, **49,** 333 – 341.
[6] Zandbergen, P. J. and Dijkstra, D., 1987, Von Karman swirling flows. *Ann. Rev. Fluid Mech.*, **14**, 465 – 491.
[7] Soo, S. L., 1958, Laminar flow over an enclosed rotating disk. *Trans. ASME*, **80**, 287 – 296.
[8] Maroti, L. A., Deak, G. and Kreith, F., 1960, Flow phenomena of partially enclosed rotating disks. *ASME J. of Basic Engineering.*, **82**, 539 – 552.
[9] Daily, J. W. and Nece, R. E., 1960, Chamber dimension effects on induced flow and frictional resistance of enclosed rotating disks. *ASME J. of Basic Eng.,* **82**, 217 – 232.
[10] Rice, W., 1963, An analytical and experimental investigation of multiple disk pumps and compressors. *ASME J. of Eng. for Power*, **85**, 191 – 200.
[11] Haisnger, S. H. and Kerhrt, L. G., 1963, Investigation of a shaer-force pump. *ASME J. of Eng. for Power*, **85**, 201 – 212.
[12] Stenning, A. H., 1956, Stall propagation in axial compressors. *NACA TN*, **3580**.
[13] Emmons, H. W., Kronauer, R. E. and Rocket, J.A., 1959, A survey of stall propagation-experimental and theory. *ASME J. of Basic Eng.*, **81**, 409 – 416.
[14] Jansen, W., 1964, Rotating stall in a radial vaneless diffuser. *ASME J. of Basic Eng.*, **86**, 750 – 758.
[15] Ohuchida, S., Kawakubo, T. and Tamaki, H., Experimental study of rotating stall in vaneless diffuser of a centrifugal compressor, Proceedings of the ASME Turbo Expo, 6C(2013), pp. 1 – 8.
[16] Lennemann, E., 1974, Aerodynamic aspects of disk files. *IBM J. Res. Develop.*, **18**, 480 – 488.
[17] Abrahamson, S. D., Eaton, J. K. and Koga, D. J., 1989, The flow between shrouded corotating disks. *Physics of Fluids A*, **1**, 241 – 251.
[18] Schuler, C. A., Usry, W. R., Humphrey, J. A. C. and Greif, R., 1990, On the flow in the unobstructed space between shrouded corotating disks. *Physics of Fluids A*, **2**, 1760 –1770.
[19] Funaki, J and Yano H., 1992, The gap flow between coaxial rotating disks. flow, 10, 274-280.
[20] Funaki, J.,Takizawa, K., Hirata, K. and Yano H., 1995, Flow modes in gap between coaxial rotating disks. *Transactions of the Japan Society of Mechanical Engineers, Series B*, **94**, 2924 – 2928 (in Japanese).
[21] Humphrey, J. A. C., Schuler, C. A. and Webster, D. R., 1995, Unsteady laminar flow between a pair of disks corotating in a fixed cylindrical enclosure, *Physics of Fluids*, **7**, 1225 – 1240.
[22] Herrero, M. A. S. J., Giralt, F. and Humphrey, J. A. C., 1999, Influence of the geometry on the structure of the flow between a pair of corotating disks. *Physics of Fluids*, **11**, 88–96.
[23] Randriamapianina, A., Schiestel, R. and Wilson, M., 2001, Spatio-temporal behaviour in an enclosed corotating disk pair. *J. Fluid Mech*., **434**, 39 – 64
[24] Hirata, K., Funaki, J., Nishida, Y., Honma, S., Yoshida, H. and Furue, M., 2006, On selection of flow modes between rotating disks. *Transactions of the Japan Society of Mechanical Engineers, Series B*, **72**, 3066 – 3073 (in Japanese).
[25] Hirata, K., Sakamoto, A., Kitagawa, A., Uno, T. and Funaki, J., 2011, On the influence of hub upon flow between co-rotating disks. *Transactions of the JSME, Series B*, **77**, 1920 – 1932 (in Japanese).
[26] Washizu, T., Lubisch, F. and Obi, S., 2013, LES study of flow between shrouded co-rotating disks. *Flow, Turbulence and Combustion*, **91**, 607-621.
[27] Uenishi, R., Tsugawa, S., Maeda, T., Uesaka, M., Watanabe, T., Tanigawa, H. and Hirata, K, 2016, Visualization of Diverse Flows between Co-Rotating Disks in Casing by Numerical Analysis and Experiment, *The 7th TSME International Conference on Mechanical Engineering.*